PCCP

Accepted Manuscript

This article can be cited before page numbers have been issued, to do this please use: J. de Ruiter and F. Buda, *Phys. Chem. Chem. Phys.*, 2016, DOI: 10.1039/C6CP07454E.

ROYAL SOCIETY OF CHEMISTRY

rsc.li/pccp

View Article Online
DOI: 10.1039/C6CP07454E

Introducing a closed system approach for the investigation of chemical steps involving proton and electron transfer; as illustrated by a copper-based water oxidation catalyst

J.M. de Ruiter[a], F. Buda[a]

[a] Leiden University, Leiden Institute of Chemistry, Einsteinweg 55, 2300 RA, Leiden, The Netherlands

Abstract

The investigation of the catalytic mechanism of homogeneous water oxidation catalysts remains an active field of research. When examining catalytic steps theoretically, it is often difficult to account for the transfer of protons and electrons from step to step. To this end, a closed system approach is proposed which includes both proton and electron acceptors in the simulation box to allow for the description of proton-coupled electron transfer processes. Using Car-Parrinello Molecular Dynamics, a mononuclear copper water oxidation catalyst $Cu(bpy)(OH)_2$ was used as a model system to explore this closed system approach. The exploration of this model system shows that, compared to traditional methods, this approach offers extra insight into proposed catalytic steps and allows to clearly identify preferred reaction paths.

View Article Online
DOI: 10.1039/C6CP07454E

Introduction

To ameliorate the impending energy crisis, abundant renewable energy sources will be needed. One of the possible solutions is the conversion of solar energy directly into fuel by means of artificial photosynthesis, using an artificial leaf. [1–4] A key component of the artificial leaf is the water oxidation catalyst, the optimisation of which is an active field of research especially using abundant transition metals such as copper and iron. [5–17] One way of optimising a proposed water oxidation catalyst is to consider its catalytic cycle and ensuring that it is as favourable as possible with low overpotential. [18,19]

Traditionally, catalytic cycles are examined computationally by comparing the free energies of the proposed catalytic intermediates and then, usually, assigning the thermodynamically most favourable cycle as the most likely catalytic cycle. [12,14,20–23] This examination often uses an implicit solvent model or correction factors to account for protons and electrons removed in the catalytic step itself,[14,20,22,24–26] while the more involved methods which do include explicit solvent molecules are very time-consuming.[27–29] Using correction factors prevents direct comparisons of the intermediates as the compared intermediates usually contain differing numbers of protons and electrons. In the case of proton-coupled electron transfer (PCET) processes,[30] it is also becoming increasingly clear that explicit solvent molecules are needed to obtain realistic descriptions of reaction pathways.[31–33] Furthermore, static considerations of reaction pathways also limit the information that can be acquired about the kinetic bottlenecks between one catalytic intermediate and the next. Dynamical insight into PCET reactions can be very useful in the design of an optimised water oxidation catalyst.

We therefore propose a closed system approach (CSA) in which the catalytic step itself can be examined, with the charge carriers being contained within the system to allow for the analysis of the free energy profile from one catalytic intermediate to the next. To test the applicability of this CSA we compare two trial catalytic cycles (see Figure 1) for the [Cu(bpy)$(OH)_2$] copper based catalyst (denoted [*Cu*$(OH)_2$]).[11] This catalyst has been reported to be active at high pH at which it has the [*Cu*$(OH)_2$] form.[11] Although the catalytic cycle of the [*Cu*$(OH)_2$] catalyst has been briefly considered theoretically,[24] a number of open questions remain. After performing a thermodynamic analysis of the two cycles based on density functional theory (DFT) calculations, the crucial O – O bonding step of Cycle 2 is examined using *ab initio* constrained molecular dynamics in explicit solvent. This explicit solvent examination is furthered by a closed system analysis using constrained molecular dynamics. The closed system approach is also used to investigate the O – O bonding step of Cycle 1. For this step an examination of the mean constraint force is also performed.

View Article Online
DOI: 10.1039/C6CP07454E

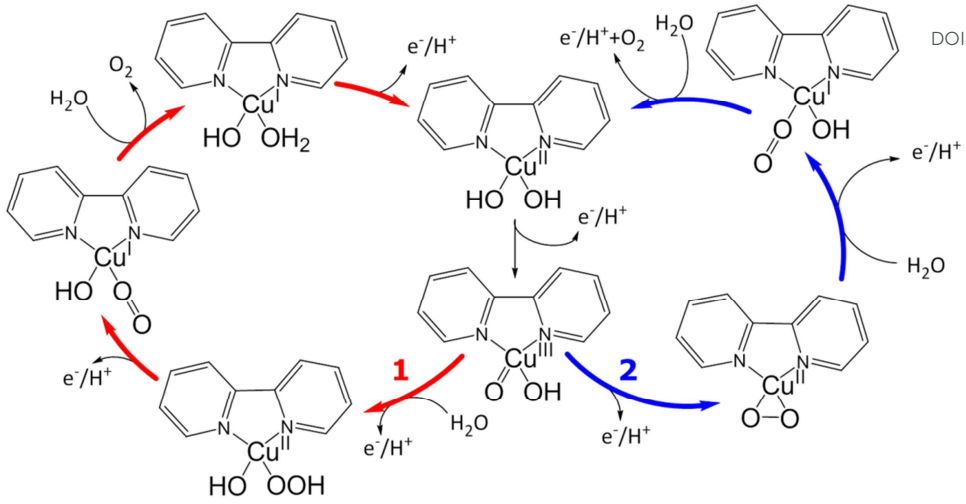

Figure 1 Two proposed mechanisms for water oxidation by [Cu(bpy)(OH)$_2$] : Cycle 1 (left) and Cycle 2 (right).

Computational method and details

Geometry optimisations and thermodynamic calculations are performed for each catalytic intermediate with DFT using the implementation in the Amsterdam Density Functional (ADF) software package.[34–36] Van der Waals interactions are accounted for by using the Grimme3 BJDAMP dispersion correction.[37] The geometries of the examined molecules are initially optimised using the OPBE functional,[38] with the TZP (triple zeta polarized) basis set and a small core. This GGA functional has shown good performance when describing transition metal complexes. [32,39–42] Benchmark studies of proton transfer energies with GGA functionals show that reaction barriers are underestimated by around 3 to 3.5 kcal mol^{-1} when compared to those calculated with highly correlated *ab initio* methods.[43] However, as we have argued earlier,[44] within CPMD this is likely compensated by the quantum effect error resulting from the classical treatment of proton motion. Comparisons between the optimised geometry of [*Cu*(OH)$_2$] with the crystal structure of a catalyst with a similar metal centre are included in the Supplementary Information (SI, Table S1).[45] These show good agreement, with OPBE/TZP reproducing most metal centre geometric parameters within a few percent. For each of the intermediates the most energetically favourable spin state is determined (see SI, Table S2). The geometric information for these intermediates is also shown in the SI, Table S3.

The thermodynamics of the catalytic cycle is obtained by calculating the Gibbs free energy difference between each catalytic intermediate following the strategy first proposed by Norskov and co-workers.[46,47] The structure of each intermediate is further optimised at the B3LYP/TZP level, in vacuum. Zero-point energy and entropic contributions are included through vibrational analysis performed with the same computational set-up. For every structure optimised in vacuum, solvation effects are accounted for by performing a single point calculation with the B3LYP functional in a water environment simulated with the COSMO model.[48] The reaction energies, zero-point energies and entropies of O_2, H_2 and H_2O are also calculated. In the case of PCET steps, the free energies of the proton and electron are included as a pair: $H^+ + e^- \rightarrow ½\ H_2$,

The CPMD program for *ab initio* molecular dynamics (MD) was used to examine the explicitly solvated systems.[49] The solvent environment for the CPMD simulations was generated using Discovery Studio 2.5.[50] The solvent was equilibrated using the CHARMM force field and CFF partial

charge parameters at 300 K,[51] while the catalyst was kept fixed. The volume was then adjusted using constant pressure, after which the system was further allowed to evolve with constant volume. Subsequently CPMD calculations were performed at 300 K, using GTH pseudopotentials for the transition metals,[52] and dispersion-corrected pseudopotentials (DCACP) for the remaining atoms,[53] and the OPBE exchange-correlation functional.[54] An energy cut-off of 70 Ry was used and a time step of 5 a.u. (1 a.u. = 0.0242 fs). Image rendering for the CPMD output was done using VMD.[55,56]

The catalytic reaction steps investigated may be considered rare events: these reactions are indeed unlikely to occur spontaneously during the standard time scale of *ab initio* MD simulations (few ps). In order to investigate these reactions, we employ a constrained MD method for rare events.[57–59] By constraining a reaction coordinate (in this case the distance between two atoms) at fixed values along a reaction path, the time-averaged constraint force for each of these values is obtained. This time-averaged constraint force is equal to zero at an equilibrium or transition state, and may be integrated to give the free energy change along the reaction path.[59,60] It should be noted that the time-scale of the events observed using this methodology will not be comparable with experiment, though the reaction rate can be extracted using transition state theory.[61] In this work, the focus is more on comparing the thermodynamics of alternative reaction paths. Three different solvated systems were investigated:

System 1

The [*Cu*(O)(O)] intermediate ($17.7 \times 17.2 \times 8.5$ Å^3 box with 73 water molecules, total charge 0, triplet multiplicity). This system is used to examine constrained molecular dynamics of the O – O bonding step of Cycle 2 in explicit solvent. A solvent water molecule is constrained at increasingly closer distances (3.82 – 1.95 Å) to the copper centre. For each distance the system is allowed to evolve for 242 fs, during which the mean constraint force is seen to stabilise. This constraint analysis is repeated constraining the distance (2.45 – 1.44 Å) between a solvent water molecule and an oxo ligand. After the constrained dynamics calculation at the shortest distance, the constraint is released and the dynamics allowed to continue for 968 fs.

System 2

The [*Cu*(O)(O)] intermediate and an Fe atom ($17.6 \times 14.9 \times 10.3$ Å^3 box with 72 water molecules, total charge 3^+, quintet or septet multiplicity).This closed system analysis using constrained molecular dynamics is performed on [*Cu*(O)(O)] to further the explicit solvent examination of the O – O bonding step of Cycle 2.The distance between a solvent water molecule and an oxo ligand is constrained at 2.3 Å and the system allowed to evolve for 1.21 ps.

System 3

The [*Cu*(OH)(O)] intermediate and an Mn atom ($17.6 \times 14.9 \times 10.3$ Å^3 box with 72 water molecules, total charge 3^+, quintet or septet multiplicity).This closed system analysis is performed to investigate the O – O bonding step of Cycle 1.The distance between a solvent water molecule and an oxo ligand is constrained at varying distances (2.4 – 1.44 Å) and the system allowed to evolve for 1.21 ps per distance.

In Systems 2 and 3 (those with an extra metal atom), a spin constraint is applied such that the number of unpaired electrons remains fixed (either 4 or 6, corresponding to a quintet or septet multiplicity) during the simulation. This results in modifying the number of unpaired spins localised on the catalyst and metal atom. A posteriori, the localisation of spin density (or lack thereof) on the

View Article Online
DOI: 10.1039/C6CP07454E

catalyst may be used to confirm the expected transfer of an electron. We also perform an integration of the spin density in two different regions of the simulation box and in this way quantitatively verify that the expected number of unpaired electrons is found on the catalyst and the extra metal atom, respectively. An Fe or Mn atom is used depending on the spin state of the to-be-investigated catalytic intermediate. These elements are selected because of their stability in either 2^+ or 3^+ oxidation states, and their differing multiplicities. By constraining the multiplicity of the system, the charge of the metal atom can be switched between the 2^+ and 3^+ state, allowing the oxidised catalyst to be directly compared to the neutral catalyst (see Equation (1), where Me denotes the additional metal ion and H_s^+ the dissociated proton in solution).

$$Me^{3+} + [Cu^{II}(OH)_2]^0 \rightleftharpoons Me^{2+} + [Cu^{III}(OH)(O)]^0 + H_s^+ \quad (1)$$

This is then the proposed closed system approach (CSA). Including explicit water in the simulation box allows for proton transfer from the catalyst to the solvent, while including a metal ion allows for the 'transfer' of an electron within the system. Here transfer is noted in inverted commas as the localisation of the electron *is* constrained by the multiplicity of the whole system. This also renders the effect of the metal's oxidation potential on electron transfer negligible. However, this set-up does allow for the analysis of the featured catalyst both before and after a supposed electron transfer within the system.

Results and Discussion

Thermodynamics of the Catalytic Cycles

We examine two trial catalytic cycles (see Figure 1) thermodynamically by calculating the free energies of each intermediate in the cycles. The two cycles are composed of PCET steps and differ primarily in the approach to the oxygen-oxygen bond formation step: Cycle 1 proceeds via nucleophilic attack while Cycle 2 features an intra-molecular O – O coupling step. These two approaches have emerged from within the natural photosynthesis community,[62,63] and have also gained traction within the artificial photosynthetic field.[12,32,64,65] It is therefore apt to compare the two. Geometries of the intermediates were optimised and the most energetically favourable multiplicity for each intermediate determined as shown in the SI (Table S3). The SI also includes renderings of the spin density of the relevant proposed intermediates (Figure S1). The changes in free energy along the trial catalytic cycles are shown in Table 1 and in the SI, Figure S2.

Table 1 Calculated ΔG for each catalytic step along the two proposed mechanisms for [Cu(bpy)(OH)$_2$] ([*Cu*(OH)$_2$])

Cycle 1	ΔG_{calc} (eV)	Cycle 2	ΔG_{calc} (eV)
[*Cu*(OH)$_2$] → [*Cu*(OH)(O)]	2.28	[*Cu*(OH)$_2$] → [*Cu*(OH)(O)]	2.28
[*Cu*(OH)(O)] → [*Cu*(OH)(OOH)]	1.27	[*Cu*(OH)(O)] → [*Cu*(O)(O)]	0.86
[*Cu*(OH)(OOH)] → [*Cu*(OH)(OO)]	0.75	[*Cu*(O)(O)] → [*Cu*(OH)(OO)]	1.16
[*Cu*(OH)(OO)] → [*Cu*(OH)(OH$_2$)]	1.46	[*Cu*(OH)(OO)] → [*Cu*(OH)$_2$]	0.73
[*Cu*(OH)(OH$_2$)] → [*Cu*(OH)$_2$]	-0.73		

The first proposed step ([*Cu*(OH)$_2$] →[*Cu*(OH)(O)]), which the two cycles share), has a difference in free energy of 2.28 V. This is then a calculated overpotential of 1.05 V as compared to the experimentally obtained 0.75 V.[11] This step is significantly higher than the others (see Table 1),

View Article Online
DOI: 10.1039/C6CP07454E

making it the thermodynamic bottleneck. Another step with relatively high calculated change in free energy is the ligand exchange step in which water is exchanged for the formed OO ligand: [*Cu*(OH)(OO)] → [*Cu*(OH)(OH_2)]. This apparently counters the general assumption that this exchange is thermodynamically neutral.[66] The assumption is based on the two ligands both being neutral. However, in this case, the Cu^{I} centre can donate some of its excess charge to the OO ligand, which more readily accepts excess electrons than the OH_2 ligand. This would then make the OO ligand slightly negatively charged, which would electrostatically stabilise this intermediate. This electrostatic attraction is also observed in the shorter Cu – O distance: 2.11 Å in [*Cu*(OH)(OO)] and 2.20 Å in [*Cu*(OH)(OH_2)]. Considering the high pH at which this catalyst oxidises water,[11] it is likely that the OO ligand exchange with a water molecule is concerted with an immediate PCET step, as per the [*Cu*(OH)(OO)] → [*Cu*($(OH)_2$] step which has a ΔG = 0.73 eV.

The differences in energies at the point where the two cycles diverge is more explicitly shown in Figure 2. In red the difference in energy for oxygen-oxygen bond formation via nucleophilic attack as per the catalytic cycle on the left in Figure 1 (Cycle 1) and in blue via intra-molecular O – O coupling as per the cycle on the right in Figure 1 (Cycle 2). The ideal difference in free energy for a water oxidation catalyst is also indicated with a grey line. Considering this step, we would expect Cycle 2 to be the more favourable as the [*Cu*(O)(O)] intermediate is energetically more favourable (0.41 eV lower than the [*Cu*(OH)(OOH)]). The two oxygens in the [*Cu*(O)(O)] intermediate strongly interact in the optimised geometry with an O – O distance of 1.47 Å. This distance is comparable to an oxygen-oxygen single bond length in, for example, hydrogen peroxide. This apparently covalent interaction between the oxygen atoms stabilises this intermediate. In order to examine how this intra-molecular O – O bond would lead to the next catalytic intermediate in the trial catalytic cycle, we move to an explicitly solvated analysis with CPMD.

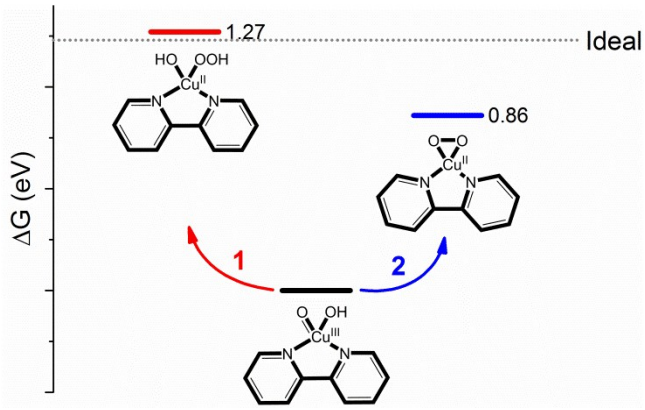

Figure 2 Difference in free energy for the two oxygen-oxygen bond formation steps: nucleophilic attack in Cycle 1 (red) and intra-molecular O – O coupling in Cycle 2 (blue) as calculated by ADF (B3LYP/TZP/COSMO). The ideal difference in free energy for water splitting is indicated by a dotted grey line.

View Article Online
DOI: 10.1039/C6CP07454E

Ab-Intio Constrained Molecular Dynamics of System 1

In System 1, which contains the [*Cu*(O)(O)] intermediate, two pathways are examined. The first is the constraining of the distance between a solvent water molecule and the copper centre, such that the water molecule approaches axially. It is hypothesised that this may displace one of the oxo ligands which, after a PCET step, would lead to the [*Cu*(OH)(OO)] intermediate as shown in Figure 1. The constrained pathway is initiated with the incoming water molecule at 3.82 Å and shortened incrementally. Little change is seen besides solvent rearrangement until the constrained distance is 1.95 Å. When constrained at 1.95 Å from the copper centre, the incoming water molecule undergoes proton transfer (see Figure 3). The proton is transferred to a ligated oxo group via another solvent molecule. This is then effectively a step backwards in the catalytic cycle as we recover the intermediate [*Cu*(OH)(O)]. The axial approach therefore does not appear to be a successful route for the formation of the intra-molecular O – O bond which would lead to the next intermediate in Cycle 2.

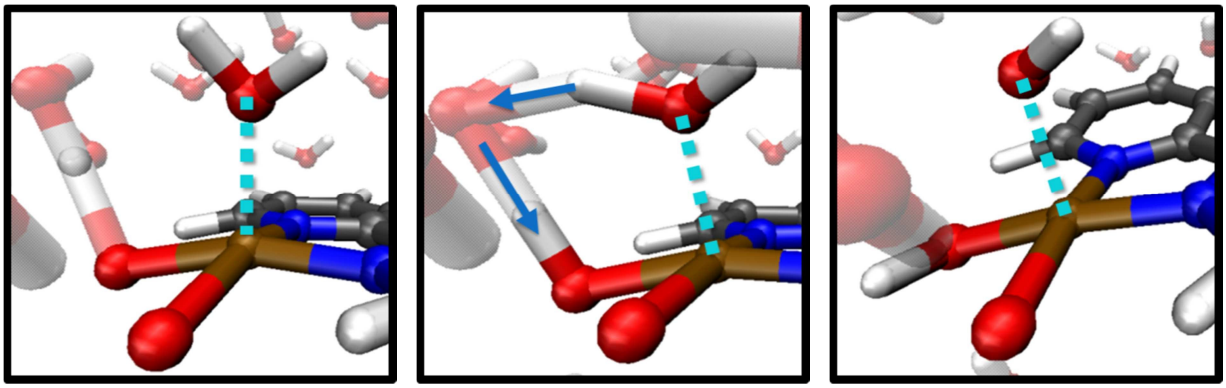

Figure 3. Subsequent snapshots of the MD simulation of System 1. A water molecule is constrained at 1.95 Å from the copper centre of the [*Cu*(O)(O)] intermediate (a) as shown by the dotted line. This intermediate then undergoes proton exchange via a solvent water molecule (b).The final conformation of the intermediate is shown in (c), where one of the oxo groups has accepted a proton.

The second pathway examined in System 1 is the approach of a water molecule to one of the oxo ligands (Figure 4). The distance between the oxygen atom of the oxo ligand and the oxygen atom of the incoming water molecule is constrained. When constrained at 1.9 Å, a proton is accepted by the oxo ligand not involved in the constraint from a solvent water molecule as shown in Figure 4(b). Once again we recover the intermediate [*Cu*(OH)(O)].

In the current set-up, the system consistently favours the formation of the [*Cu*(OH)(O)] intermediate. This may be because the oxidation state of the copper must change. In the current MD set-up proton transfer can occur from catalyst to solvent, however there is no electron acceptor which might allow for electron transfer from the catalyst. We therefore move on to the proposed CSA, which includes an additional metal ion capable of acting as an electron acceptor.

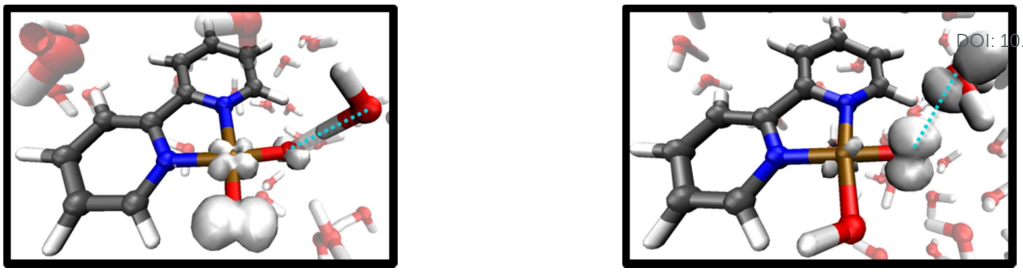

(a) (b)

Figure 4. Snapshots of an alternative pathway proposed for System 1 featuring the [*Cu*(O)(O)] intermediate. Localisation of the spin density (grey isosurface) is shown while a water molecule is constrained at increasingly shorter distances to an oxo ligand (as shown by the dotted line): d (O – O) = 2.45 Å (a) and d(O – O) = 1.9 Å (b).

Closed System Analysis of the [*Cu*(O)(O)] intermediate

In the closed system analysis of the [*Cu*(O)(O)] intermediate, a Fe metal ion is used as an electron acceptor (System 2). We start a constrained molecular dynamic pathway of a solvent water molecule approaching an oxo group, with an initial constrained O – O distance of 2.3 Å. Two cases are examined: the neutral catalyst ($[Cu]^0$ + Fe^{3+}) and the ionised one ($[Cu]^+$+ Fe^{2+}). In this way the total charge in the entire system remains constant. The 'transfer' of an electron is imposed by switching the multiplicity of the entire system from septet to quintet. After allowing the MD simulation to evolve for 1.21 ps, it is seen that in both cases – the neutral and the ionised catalyst – a proton from a solvent water molecule is accepted by the oxo group (Figure 5). This strongly suggests that the [*Cu*(O)(O)] intermediate is not stable in a solvated water environment, even if an electron has been removed from the catalyst (as shown in Figure 5: $[Cu]^+$+ Fe^{2+}).

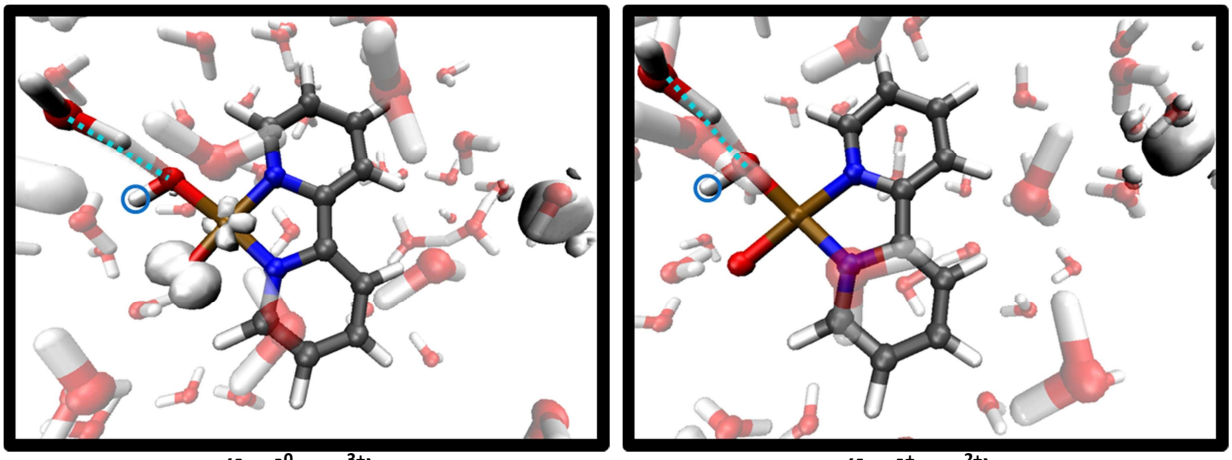

($[Cu]^0$ + Fe^{3+}) ($[Cu]^+$+ Fe^{2+})

Figure 5. Spin density (shown as a grey isosurface) of [*Cu*(O)(O)] + Fe system with septet ($[Cu]^0$ + Fe^{3+}) and quintet ($[Cu]^+$+ Fe^{2+}) multiplicity, after MD simulation. The constrained water molecule as well as the catalyst are shown in bold. The Fe ion is visible on the right hand side, enveloped by spin density. In the case of the neutral catalyst, spin density is also seen on the copper centre and oxo ligand. In the spin-flipped case ($[Cu]^+$+ Fe^{2+}), spin density is only seen on the Fe ion as expected. The total charge of the system is 3^+. In both cases, a proton (circled in blue) is accepted by an oxo ligand.

In both System 1 and System 2 solvent water molecules play a crucial role in the shuttling of protons around the catalytic site. Furthermore it appears that the thermodynamic calculations of the [*Cu*(O)(O)] intermediate without explicit water molecules led to the artificial stabilisation of an O – O bond. Although thermodynamic analysis suggested that Cycle 2 would be more favourable, in explicit solvent the [*Cu*(O)(O)] intermediate decays to the [*Cu*(OH)(O)] intermediate. Proceeding to the next

catalytic intermediate in Cycle 2 via intra-molecular O – O coupling is therefore unlikely. This highlights the need for an explicit solvent when proposing and considering catalytic cycles.

Closed System Analysis of the [*Cu*(OH)(O)] intermediate

To further explore the catalytic cycle using the proposed methodology we examine the O – O bond formation step by nucleophilic attack as proposed in Cycle 1. Using System 3 (which contains the [*Cu*(OH)(O)] intermediate and a Mn ion) a sequence of constrained MD simulations is performed with a quintet (neutral catalyst) or septet (ionised catalyst) multiplicity. The distance between the oxo ligand and the oxygen of an incoming water is constrained, and the time-averaged constraint force monitored. In this way we examine the [*Cu*(OH)(O)] intermediate as it would hypothetically react to form the [*Cu*(OH)(O)] intermediate. In Figure 6 the time-averaged constraint force of the system containing the neutral catalyst and Mn^{3+} ion ($[Cu]^0 + Mn^{3+}$) as the constraint is shortened is shown with black squares, while the system containing the ionised catalyst and Mn^{2+} ($[Cu]^+ + Mn^{2+}$) is shown with red circles. The average O – O bond length in an unconstrained MD simulation performed after the bond has been formed is also shown in Figure 6 as a green triangle. Reversing the process by breaking the recently formed O – O bond (i.e. [*Cu*(OH)(OOH)] → [*Cu*(OH)(O)]) is shown with blue triangles, while the pathway along the lowest energy intermediates is indicated in Figure 6 by a green dotted line.

At larger distances (2.4 – 2.9 Å), the $[Cu]^0 + Mn^{3+}$ system experiences less force under the constraint which corresponds to a relatively lower free energy landscape. However, between 2.4 and 2.1 Å a crossing of the two curves occurs, indicating that at distances less than ~2.35 Å the system experiences less force if the electron is found on the Mn ion rather than on the catalyst. That is to say, as soon as an incoming solvent molecule is within 2.35 Å of the oxo group of the [*Cu*(OH)(O)] intermediate, the ionised intermediate is more stable.

When the incoming water molecule is 1.7 Å from the oxo ligand of the neutral catalyst, a proton is seen to be accepted from a solvent molecule by the oxo group involved in the constraint (see Figure 7, upper panel). The same result is also obtained when starting from an unconstrained MD simulation of the final product ([*Cu*(OH)(OOH)]) having changed the multiplicity (thereby moving an electron onto the [*Cu*(OH)(OOH)] intermediate). We can therefore conclude that electron removal is indeed necessary to advance through the proposed catalytic cycle. Comparatively, when following the red points as the constrained distance is shortened, the proposed [*Cu*(OH)(OOH)] intermediate is eventually obtained (Figure 7, lower panel). The constraint is then removed and the system allowed to evolve while the bond length of the recently formed bond is monitored. This is seen to stabilise to around 1.50 Å (Figure 7, green triangle). This confirms the stability of the proposed [*Cu*(OH)(OOH)] intermediate.

View Article Online
DOI: 10.1039/C6CP07454E

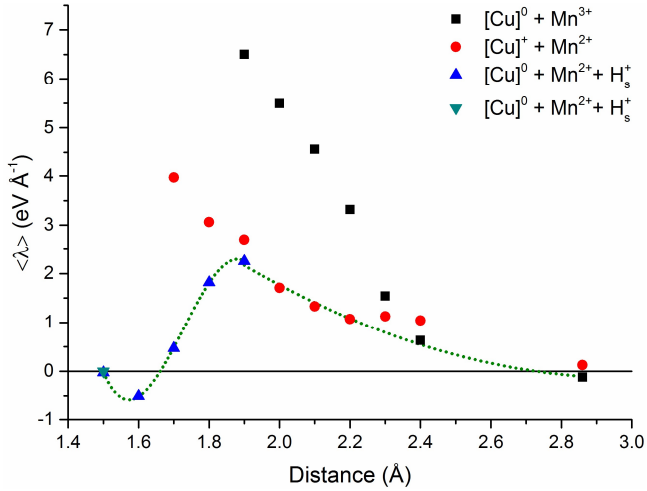

Figure 6 The time-averaged constraint force (<λ>) as a function of O – O distance as a solvent water molecule is brought increasingly closer to the oxo group of the [*Cu*(OH)(O)] intermediate (System 3). This analysis is performed for the system in quintet ($[Cu]^0$ + Mn^{3+}) and septet ($[Cu]^+$ + Mn^{2+}) multiplicity. The average distance of the O – O bond once the constraint has been released after the last $[Cu]^+$ + Mn^{2+} constrained MD is indicated by a green triangle ($[Cu]^0$ + Mn^{2+}+ H^+_s). The constrained force analysis is also done in reverse: lengthening the formed O – O bond for the system with septet multiplicity ($[Cu]^0$ + Mn^{2+}+ H^+_s). The green dotted line indicates the lowest energy pathway

Although electron transfer is seen to be favourable from an O – O distance of ~2.35 Å, proton transfer is not observed until after an O – O distance of 1.7 Å (see Figure 7, lower panel). This proton transfer is mostly dependent on solvent rearrangement. This catalytic step proceeds by the removal of an electron followed by the dissociation of a proton once the solvent has rearranged such that the proton transfer into the solvent is favourable.[44] The dependence on solvent rearrangement in these simulations also leads to a 'hysteresis' effect:[57] if the bond is lengthened from the [*Cu*(OH)(OOH)] intermediate it gives a different mean constraint force curve (blue curve in Figure 6). That the [*Cu*(OH)(O)] → [*Cu*(OH)(OOH)] might be considered the more likely step is confirmed by a similar investigation of the [*Cu*(OH)(O)] → [*Cu*(O)(O)] step as shown in the SI, Figures S3-S5.

To examine the effect of the inclusion of the metal atom, the curve produced via the lengthening of the O – O bond (i.e. [*Cu*(OH)(OOH)] → [*Cu*(OH)(O)]) is reproduced without the inclusion of the metal atom. As the electron would have already been transferred to the electron acceptor at this point, and the proton into solution, the time-averaged constraint force of this constraint should be comparable. These two curves are compared in the SI (Figure S6), and show very close agreement. The inclusion of the additional metal ion therefore has very little effect on the time-averaged constraint force, and thus the change in free energy of this bond lengthening process.

Although the CSA (in its current form) is very useful for the analysis and comparison of free energy profiles from one catalytic intermediate to the next, a direct comparison of the estimated free energy change with experimental data is still not straightforward. This is mainly due to the energetic contributions of the extra metal ion that are included within the closed system, which remain difficult to deconstruct. Future work will include an energetic calibration of this approach.

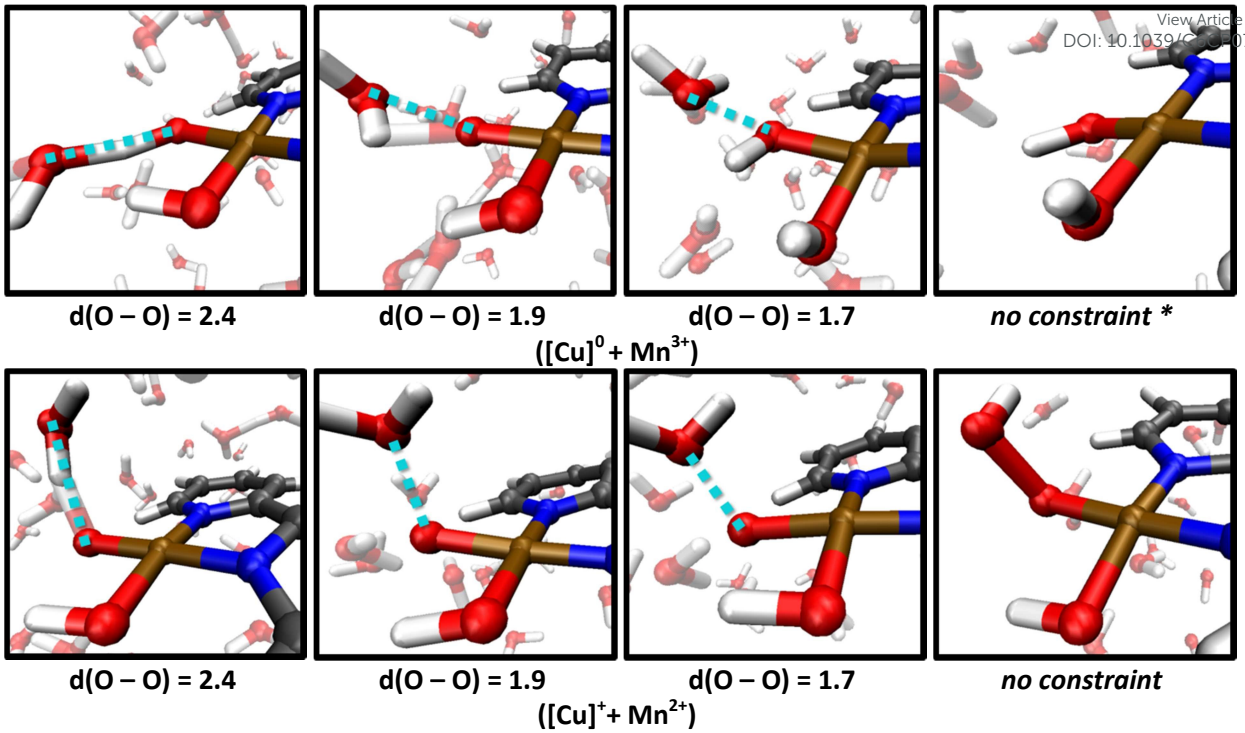

Figure 7 Snapshots taken during CPMD calculations as a solvent water molecule is constrained at increasingly shorter distance to the oxo group of the [*Cu*(OH)(O)] intermediate. *Spin flipped from ([Cu]$^{+}$ + Mn^{2+})

Conclusions

The relevant steps of two trial water oxidation catalytic cycles were analysed using a closed system approach in which an electron acceptor is included in a fully solvated simulation setup. Using this approach it is observed that the solvent acts as a proton shuttle, favouring the catalytic cycle which does not include the formation of the [*Cu*(O)(O)] intermediate (Cycle 1). This is contrary to the expectations based on the thermodynamic analysis within a COSMO model. When investigating the oxygen – oxygen formation step of Cycle 1, it is observed that this reaction proceeds by the electron leaving first, followed by proton transfer when solvent dynamics creates an appropriate hydrogen bonding network. This closed system approach provides additional insight into PCET catalytic steps by elucidating the dynamic evolution between two stable intermediates.

Acknowledgements

FB dedicates this work to Professor Evert Jan Baerends on the occasion of his 70th birthday. The use of supercomputer facilities was sponsored by NWO Physical Sciences, with financial support from the Netherlands Organization for Scientific Research (NWO). JMdR would also like to acknowledge Jan-Paul Menzel for useful discussions.

References

1 K. J. Young, L. A. Martini, R. L. Milot, R. C. Snoeberger III, V. S. Batista, C. A. Schmuttenmaer, R. H. Crabtree and G. W. Brudvig, *Coord. Chem. Rev.*, 2012, **256**, 2503–2520.
2 D. Gust, T. A. Moore and A. L. Moore, *Acc. Chem. Res.*, 2009, **42**, 1890–1898.
3 C. Liu, B. C. Colón, M. Ziesack, P. A. Silver and D. G. Nocera, *Science*, 2016, **352**, 1210–1213.
4 D. G. Nocera, *Acc. Chem. Res.*, 2012, **45**, 767–776.

5 L. Duan, F. Bozoglian, S. Mandal, B. Stewart, T. Privalov, A. Llobet and L. Sun, *Nat. Chem.*, 2012, **4**, 418–423.
6 L. Duan, C. M. Araujo, M. S. G. Ahlquist and L. Sun, *Proc. Natl. Acad. Sci.*, 2012, **109**, 15584–15588.
7 L. Duan, Y. Xu, M. Gorlov, L. Tong, S. Andersson and L. Sun, *Chem. – Eur. J.*, 2010, **16**, 4659–4668.
8 L. Tong, L. Duan, Y. Xu, T. Privalov and L. Sun, *Angew. Chem. Int. Ed.*, 2011, **50**, 445–449.
9 D. G. H. Hetterscheid and J. N. H. Reek, *Angew. Chem. Int. Ed.*, 2012, **51**, 9740–9747.
10 N. Kaveevivitchai, R. Zong, H.-W. Tseng, R. Chitta and R. P. Thummel, *Inorg. Chem.*, 2012, **51**, 2930–2939.
11 S. M. Barnett, K. I. Goldberg and J. M. Mayer, *Nat. Chem.*, 2012, **4**, 498–502.
12 J. D. Blakemore, N. D. Schley, D. Balcells, J. F. Hull, G. W. Olack, C. D. Incarvito, O. Eisenstein, G. W. Brudvig and R. H. Crabtree, *J. Am. Chem. Soc.*, 2010, **132**, 16017–16029.
13 D. J. Wasylenko, R. D. Palmer and C. P. Berlinguette, *Chem. Commun.*, 2013, **49**, 218.
14 D. E. Polyansky, J. T. Muckerman, J. Rochford, R. Zong, R. P. Thummel and E. Fujita, *J. Am. Chem. Soc.*, 2011, **133**, 14649–14665.
15 A. Savini, G. Bellachioma, G. Ciancaleoni, C. Zuccaccia, D. Zuccaccia and A. Macchioni, *Chem. Commun.*, 2010, **46**, 9218–9219.
16 L.-Z. Fu, T. Fang, L.-L. Zhou and S.-Z. Zhan, *RSC Adv.*, 2014, **4**, 53674–53680.
17 J. L. Fillol, Z. Codolà, I. Garcia-Bosch, L. Gómez, J. J. Pla and M. Costas, *Nat. Chem.*, 2011, **3**, 807–813.
18 M. T. M. Koper, *Chem. Sci.*, 2013, **4**, 2710–2723.
19 H. Dau, C. Limberg, T. Reier, M. Risch, S. Roggan and P. Strasser, *ChemCatChem*, 2010, **2**, 724–761.
20 T. Wang, G. W. Brudvig and V. S. Batista, *J. Chem. Theory Comput.*, 2010, **6**, 2395–2401.
21 M. D. Kärkäs, T. Åkermark, E. V. Johnston, S. R. Karim, T. M. Laine, B.-L. Lee, T. Åkermark, T. Privalov and B. Åkermark, *Angew. Chem. Int. Ed.*, 2012, **51**, 11589–11593.
22 A. Venturini, A. Barbieri, J. N. H. Reek and D. G. H. Hetterscheid, *Chem. – Eur. J.*, 2014, **20**, 5358–5368.
23 M. Orio, D. Pantazis and F. Neese, *Photosynth. Res.*, 2009, **102**, 443–453.
24 T. Zhang, C. Wang, S. Liu, J.-L. Wang and W. Lin, *J. Am. Chem. Soc.*, 2014, **136**, 273–281.
25 A. V. Marenich, A. Majumdar, M. Lenz, C. J. Cramer and D. G. Truhlar, *Angew. Chem. Int. Ed.*, 2012, **51**, 12810–12814.
26 J. J. Concepcion, J. W. Jurss, J. L. Templeton and T. J. Meyer, *J. Am. Chem. Soc.*, 2008, **130**, 16462–16463.
27 F. Costanzo, M. Sulpizi, R. G. D. Valle and M. Sprik, *J. Chem. Phys.*, 2011, **134**, 244508.
28 J. Cheng, M. Sulpizi and M. Sprik, *J. Chem. Phys.*, 2009, **131**, 154504.
29 J. Cheng, X. Liu, J. VandeVondele, M. Sulpizi and M. Sprik, *Acc. Chem. Res.*, 2014, **47**, 3522–3529.
30 S. Hammes-Schiffer, *Acc. Chem. Res.*, 2009, **42**, 1881–1889.
31 C. Ma, S. Piccinin and S. Fabris, *ACS Catal.*, 2012, **2**, 1500–1506.
32 J. L. Vallés-Pardo, M. C. Guijt, M. Iannuzzi, K. S. Joya, H. J. M. de Groot and F. Buda, *ChemPhysChem*, 2012, **13**, 140–146.
33 T. J. Eisenmayer and F. Buda, *ChemPhysChem*, 2014, **15**, 3258–3263.
34 C. F. Guerra, J. G. Snijders, G. te Velde and E. J. Baerends, *Theor. Chem. Acc.*, 1998, **99**, 391–403.
35 G. te Velde, F. M. Bickelhaupt, E. J. Baerends, C. Fonseca Guerra, S. J. A. van Gisbergen, J. G. Snijders and T. Ziegler, *J. Comput. Chem.*, 2001, **22**, 931–967.
36 SCM, *ADF 2012*, Theoretical Chemistry, Vrije Universiteit, Amsterdam, The Netherlands.
37 S. Grimme, S. Ehrlich and L. Goerigk, *J. Comput. Chem.*, 2011, **32**, 1456–1465.
38 M. Swart, A. W. Ehlers and K. Lammertsma, *Mol. Phys.*, 2004, **102**, 2467–2474.
39 A. R. Groenhof, A. W. Ehlers and K. Lammertsma, *J. Am. Chem. Soc.*, 2007, **129**, 6204–6209.
40 M.-S. Liao, J. D. Watts and M.-J. Huang, *J. Phys. Chem. A*, 2007, **111**, 5927–5935.
41 M. Güell, J. M. Luis, P. E. M. Siegbahn and M. Solà, *JBIC J. Biol. Inorg. Chem.*, 2009, **14**, 273–285.
42 J. M. de Ruiter, R. L. Purchase, A. Monti, C. J. M. van der Ham, M. P. Gullo, K. S. Joya, M. D'Angelantonio, A. Barbieri, D. G. H. Hetterscheid, H. J. M. de Groot and F. Buda, *ACS Catal.*, 2016, 7340–7349.

View Article Online
DOI: 10.1039/C6CP07454E

43 S. Nachimuthu, J. Gao and D. G. Truhlar, *Chem. Phys.*, 2012, **400**, 8–12.
44 A. Monti, J. M. de Ruiter, H. J. M. de Groot and F. Buda, *J. Phys. Chem. C*, 2016.
45 Bon Kweon Koo, *Bull Korean Chem Soc*, 2001, **22**, 113.
46 J. K. Nørskov, J. Rossmeisl, A. Logadottir, L. Lindqvist, J. R. Kitchin, T. Bligaard and H. Jónsson, *J. Phys. Chem. B*, 2004, **108**, 17886–17892.
47 J. Rossmeisl, A. Logadottir and J. K. Nørskov, *Chem. Phys.*, 2005, **319**, 178–184.
48 A. Klamt, *COSMO-RS: From Quantum Chemistry to Fluid PhaseThermodynamics and Drug Design*, Elsevier Science, Amsterdam, 2005.
49 *CPMD*, Copyright IBM Corp 1990-2008, Copyright MPI für Festkörperforschung Stuttgart 1997-2001.
50 "Accelrys Software Inc.," *Discovery Studio Modeling Environment*, Accelrys Software Inc., San Diego, San Diego, 2012.
51 B. R. Brooks, R. E. Bruccoleri, B. D. Olafson, D. J. States, S. Swaminathan and M. Karplus, *J. Comput. Chem.*, 1983, **4**, 187–217.
52 C. Hartwigsen, S. Goedecker and J. Hutter, *Phys. Rev. B*, 1998, **58**, 3641–3662.
53 I.-C. Lin, M. D. Coutinho-Neto, C. Felsenheimer, O. A. von Lilienfeld, I. Tavernelli and U. Rothlisberger, *Phys. Rev. B*, 2007, **75**, 205131.
54 I.-C. Lin, M. D. Coutinho-Neto, C. Felsenheimer, O. A. von Lilienfeld, I. Tavernelli and U. Rothlisberger, *Phys. Rev. B*, 2007, **75**, 205131.
55 W. Humphrey, A. Dalke and K. Schulten, *J. Mol. Graph.*, 1996, **14**, 33–38.
56 *VMD - Visual Molecular Dynamics*, .
57 B. Ensing, E. J. Meijer, P. E. Blöchl and E. J. Baerends, *J. Phys. Chem. A*, 2001, **105**, 3300–3310.
58 F. Costanzo and R. G. Della Valle, *J. Phys. Chem. B*, 2008, **112**, 12783–12789.
59 M. Sprik and G. Ciccotti, *J. Chem. Phys.*, 1998, **109**, 7737–7744.
60 W. K. den Otter and W. J. Briels, *J. Chem. Phys.*, 1998, **109**, 4139–4146.
61 D. Frenkel and B. Smit, *Understanding Molecular Simulation: From Algorithms to Applications*, Academic Press, California, 2nd edn., 2001.
62 D. J. Vinyard, S. Khan and G. W. Brudvig, *Faraday Discuss.*, 2015, **185**, 37–50.
63 P. E. M. Siegbahn, *Philos. Trans. R. Soc. Lond. B Biol. Sci.*, 2008, **363**, 1221–1228.
64 F. Acuña-Parés, Z. Codolà, M. Costas, J. M. Luis and J. Lloret-Fillol, *Chem. - Eur. J.*, 2014, **20**, 5696–5707.
65 L. Vilella, P. Vidossich, D. Balcells and A. Lledós, *Dalton Trans.*, 2011, **40**, 11241–11247.
66 J. Rossmeisl, Z.-W. Qu, H. Zhu, G.-J. Kroes and J. K. Nørskov, *J. Electroanal. Chem.*, 2007, **607**, 83–89.